JOURNAL OF GUIDANCE, CONTROL, AND DYNAMICS
Vol. 22, No. 1, January–February 1999

Independent Analysis of the Space Station Node Modal Test Data

Richard S. Pappa*
NASA Langley Research Center, Hampton, Virginia 23681

With complex structures, comparison of independently derived sets of experimental modal parameters is an excellent way to increase confidence in the results. Modal identification results are presented using the eigensystem realization algorithm on frequency response functions from the modal test of the space station resource node. The resource node is the first U.S.-built structure for the International Space Station. The modal test was conducted by the NASA Marshall Space Flight Center in January 1997 for The Boeing Company, who designed and built the node. The calculated parameters are compared with independent results obtained by the test team using commercial software. There was excellent correlation of mode shapes between the two sets of results for the first 21 vibration modes of the structure up to 35 Hz. From 35 to 50 Hz, about 60% of 25 additional modes had excellent correlation. Natural frequencies and damping factors of most modes agreed within 0.1 Hz and 0.2%, respectively.

Introduction

BEGINNING with the launch of the Russian-built, U.S.-financed, functional cargo block (FGB) in November 1998, a consortium of 15 nations will begin assembly of the International Space Station (ISS), the largest scientific cooperative program in history.† (Note: throughout the space station program, the functional cargo block is referred to as the FGB, which is the acronym of the Russian translation of the name.) The components of the ISS will be ferried to space over a period of approximately five years in 44 separate missions using both U.S. and Russian launch vehicles. At completion, the ISS will have a width (wingspan) of 356 ft, a length of 290 ft, and a mass of nearly 1×10^6 lb. The pressurized interior is more than 46,000 ft^3, roughly equivalent to the passenger cabin volume of two 747 jetliners. It will provide living and working space for up to seven full-time occupants.

One month after the FGB is placed into orbit, the Space Shuttle will bring up the second component of the ISS known as resource node number 1. It is a pressurized, cylindrical hub approximately 17.5 ft long and 14 ft in diameter with four radial ports and two axial ports. Attached to each axial port is an 8-ft-long pressurized mating adapter (PMA) tunnel. One of the PMAs is the connecting passageway between the U.S. and Russian areas of the station. The other end of the node will eventually connect to the U.S. laboratory module. The radial ports provide additional attachment points for other structures including the U.S. habitation module at the nadir port.

Figure 1 shows how the resource node will be attached to the FGB on Shuttle mission STS-88 in December 1998. The node rides to space longitudinally in the cargo bay of the Space Shuttle and is then rotated and remounted laterally by the robotic arm. The Orbiter will then rendezvous with the FGB as shown. Connection occurs by mating the exposed upper end of the PMA with the axial docking port of the FGB.

The resource node and the PMAs were designed and built under contract to NASA by the Boeing Company. In January 1997, the Dynamics Test Branch at the NASA Marshall Space Flight Center (MSFC), in collaboration with Boeing, conducted an extensive modal test of the node at MSFC to validate the structural analytical model in accordance with NSTS 14046 and SSP 30599 (Refs. 1 and 2). The structure was mounted in a massive test fixture that constrained it in a manner similar to the boundary conditions of the Shuttle cargo bay. Using commercially available software, the test team identified 45 modes of vibration from 0 to 50 Hz (Ref. 3).

Prior to receiving the MSFC report containing their test results,[4] the NASA Langley Research Center (LaRC) performed an independent modal analysis of the same set of frequency response functions (FRFs) using their in-house-developed eigensystem realization algorithm (ERA).[5,‡] LaRC received these FRFs as a test case for ongoing research in the area of autonomous structural modal identification.[6] These data, one of the largest sets of FRFs ever measured in a modal test, were analyzed with the latest version of the autonomous ERA procedure, and the results are presented in this paper. The paper also compares the experimental modal parameters obtained by each of the two organizations.

The following section briefly describes the test structure and the test procedure. Typical FRF data and corresponding mode indicator functions appear in the next section to show the quality and complexity of the measurements. The remainder of the paper summarizes the ERA results and compares them with the test team results.

Test Article and Test Procedure

Figure 2 shows the resource node installed in the modal test stand at MSFC. This is the launch configuration of mission STS-88. The structure is held in place by four trunnions (two on each side) and a keel fitting at the bottom. The PMAs attached to the axial ports of the node are not flight hardware, but are simple mass simulators. The node was thoroughly instrumented with 1236 accelerometers consisting of 412 triaxial locations, as shown in Fig. 3. Three shakers located at the aft end of the payload excited it in each of the x, y, and z directions. Note in Fig. 3 that there are several internal instrumented components. The internal elements are four forward and four aft endcone support structures, four alcove and four midbay support structures, and one standard space station instrumentation rack. Each of the five Shuttle attachment points is also heavily instrumented with triaxial accelerometers.

The structure was excited with uncorrelated, burst-random excitation by all three shakers simultaneously. A 224-channel data acquisition system measured the accelerometer signals in six sequential data sets. For each data set the shakers ran for approximately 55 min to generate FRFs with 100 ensemble averages. There is a total of 3708 FRFs (3×1236), each having 1600 lines of resolution up to 50 Hz.

Data Overview

Figure 4 shows a typical acceleration/force FRF. This is the driving-point measurement for the x-direction shaker. Note that the

Received Dec. 9, 1997; revision received June 20, 1998; accepted for publication July 4, 1998.

*Research Engineer, Structural Dynamics Branch, Structures Division.

†Lewis, R. E., "International Space Station," Web site: http://station.nasa.gov, Aug. 1998.

‡Pappa, R. S., "Eigensystem Realization Algorithm Bibliography," Web site: http://sdb-www.larc.nasa.gov/SDB/Research/data/ERA_biblio.html, June 1998.

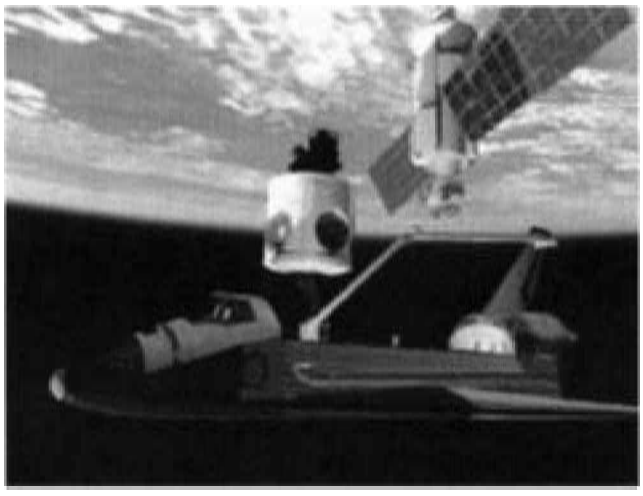

Fig. 1 Assembly in space of the node and FGB.

Fig. 2 Modal test configuration.

phase angle oscillates entirely between 0 and 180 deg because the excitation and response degrees of freedom coincide. This FRF displays approximately 25 resonances from 8 to 50 Hz. (There are none below 8 Hz.) However, the structure has about 45 modes of vibration in this bandwidth. The other modes are indistinguishable in the plot because either they were not excited by this particular shaker or they are too close in frequency to another mode to be observed.

A better way to determine the number of modes in this frequency range is by counting the dips in the multivariate mode indicator function (MMIF).[7] Because there were three shakers in the test, there are three indicator functions: primary, secondary, and tertiary.

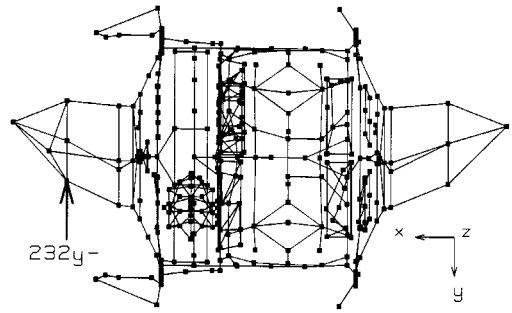

a) Top view

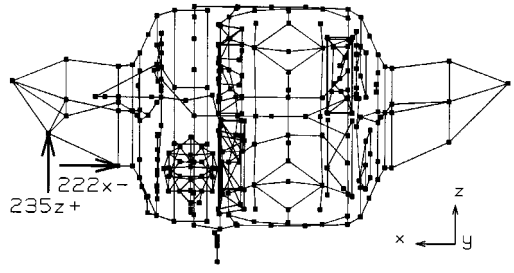

b) Side view

Fig. 3 Excitation and response locations (3 shakers and 412 triaxial accelerometers).

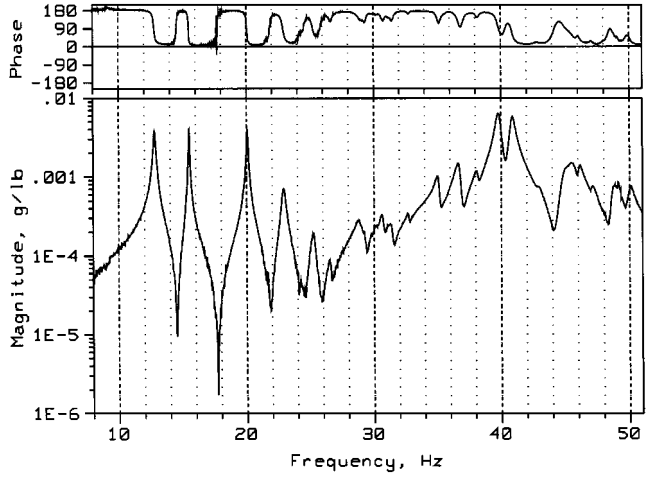

Fig. 4 Driving-point frequency response.

These functions derive from the complete set of FRFs by solving a third-order eigenvalue problem at each of the 1600 frequency lines. Figure 5 shows the primary and secondary MMIFs. The tertiary function is not plotted because it contains no significant additional information. Because of the relatively low damping of the structure, as well as the high resolution of the measurements, the primary indicator function dips sharply and deeply at each mode. The secondary indicator function dips at frequencies where additional, closely spaced modes occur.

To a significant degree, the MMIF results in Fig. 5 indicate reliably and precisely the natural frequencies of the modes of vibration. However, they provide no corresponding mode shape or damping information. Also, there is a fair amount of uncertainty concerning the number of modes in those frequency intervals with overlapping and/or shallow dips.

ERA Modal Identification Results

ERA is a multiple-input/multiple-output, time-domain technique that uses all available frequency response functions simultaneously to calculate the natural frequencies, damping factors, and mode shapes of a structure, i.e., its modal parameters.[5,6,8,‡] Figure 6 shows

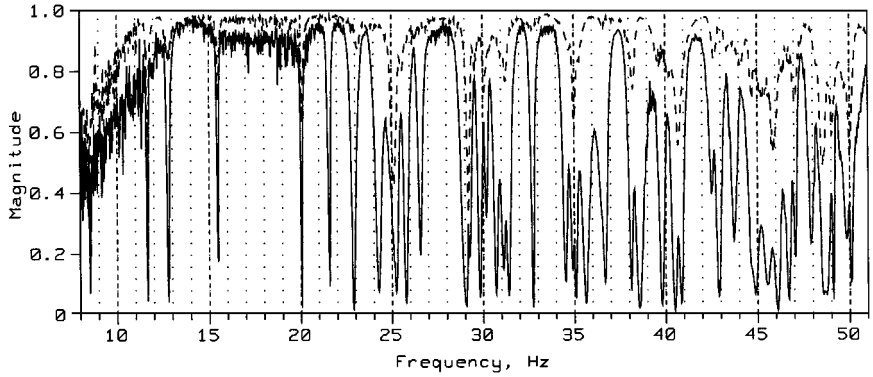

Fig. 5 Mode indicator functions: ——, primary, and – – –, secondary.

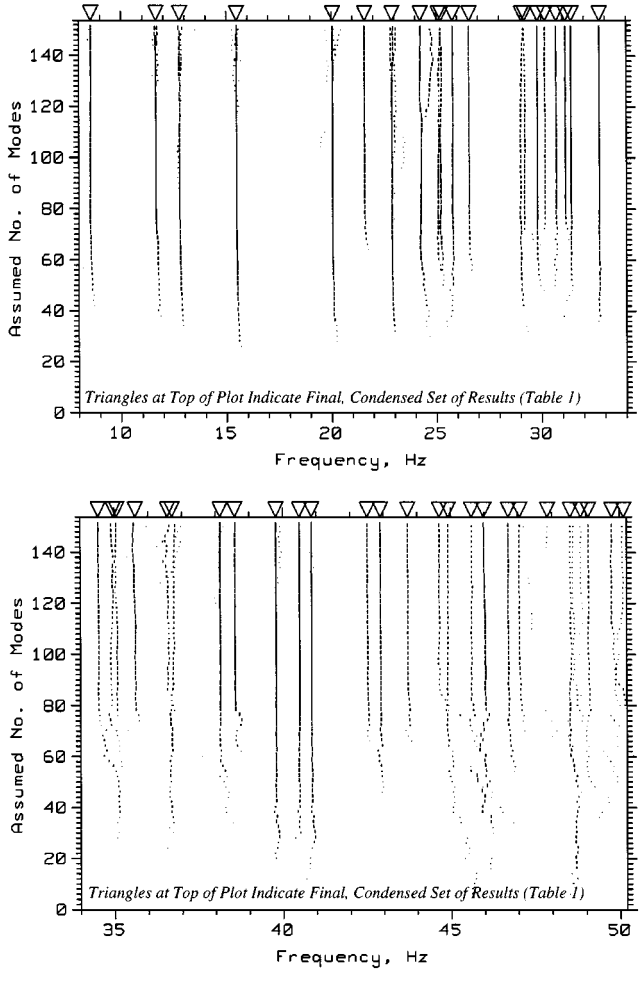

Fig. 6 ERA-identified natural frequencies vs assumed number of modes.

the results obtained by analyzing the entire set of 3708 FRFs simultaneously using a wide range of assumed number of modes from 2 to 150 in steps of 2. The specific ERA equations used in this application appear in the Appendix. Each row of results in Fig. 6 shows the set of ERA-identified natural frequencies obtained with the specified number of assumed modes. (There is a total of 75 rows.) Each identified mode is represented by a short vertical dash at the associated frequency. The height of the dash is directly proportional to the consistent-mode indicator (CMI), the principal accuracy indicator of ERA.[8] Modes with CMI values greater than approximately 80% are identified with high confidence. Modes with values ranging from 80% to 1% display moderate to large uncertainty. Fictitious computational modes have values of approximately zero. For clarity, the plots exclude all results with CMI values less than 10%.

Table 1 ERA results

Mode no.	Frequency, Hz	Damping factor, %	CMI, %	MPC-W, %
1	8.562	0.358	95.5	97.3
2	11.651	0.342	97.2	99.2
3	12.776	0.600	96.3	98.6
4	15.481	0.191	98.7	99.5
5	20.059	0.259	94.9	95.8
6	21.583	0.348	87.9	97.4
7	22.888	0.594	93.8	98.3
8	24.245	0.941	95.4	99.0
9	25.093	0.622	89.2	97.6
10	25.221	0.763	91.5	98.7
11	25.781	0.686	93.5	97.2
12	26.565	0.579	90.7	98.9
13	29.045	0.857	76.7	94.7
14	29.182	0.574	77.7	94.0
15	29.810	0.500	90.7	95.0
16	30.159	0.519	78.9	88.1
17	30.699	0.543	92.5	96.2
18	31.131	0.500	92.4	97.7
19	31.404	0.532	94.8	97.2
20	32.732	0.313	97.6	99.7
21	34.524	0.509	86.7	97.6
22	34.970	0.291	78.0	86.2
23	35.074	0.428	75.1	81.8
24	35.621	0.515	83.9	96.4
25	36.573	0.727	59.5	72.6
26	36.708	0.348	80.0	90.8
27	38.132	0.419	92.1	97.7
28	38.570	0.390	94.9	99.9
29	39.796	0.503	94.0	95.6
30	40.495	0.607	94.7	98.3
31	40.859	0.488	95.9	97.2
32	42.512	0.509	79.3	98.8
33	42.904	0.521	88.8	98.5
34	43.716	0.692	68.9	95.7
35	44.657	0.349	73.4	95.0
36	44.928	0.747	58.5	68.5
37	45.622	1.015	58.0	77.5
38	45.983	0.401	90.8	97.6
39	46.710	0.426	76.4	86.4
40	47.046	0.366	61.6	79.0
41	47.870	0.923	10.9	58.3
42	48.540	0.482	25.7	32.2
43	48.852	1.110	12.7	23.7
44	49.077	0.297	56.3	71.7
45	49.762	0.564	62.5	84.4
46	50.109	0.462	22.0	60.9

Note that Fig. 6 is divided into two frequency bands (8–34 and 34–50 Hz). This is done for plotting purposes only. Each of the 75 ERA cases generated the complete set of frequencies shown. The plots begin at 8 Hz because there are no modes below this frequency. The plots extend to slightly above 50 Hz, the maximum frequency of interest.

A mode with a CMI of 100% has a vertical dash height in Fig. 6 equal to the distance between minor tic marks on the *y*

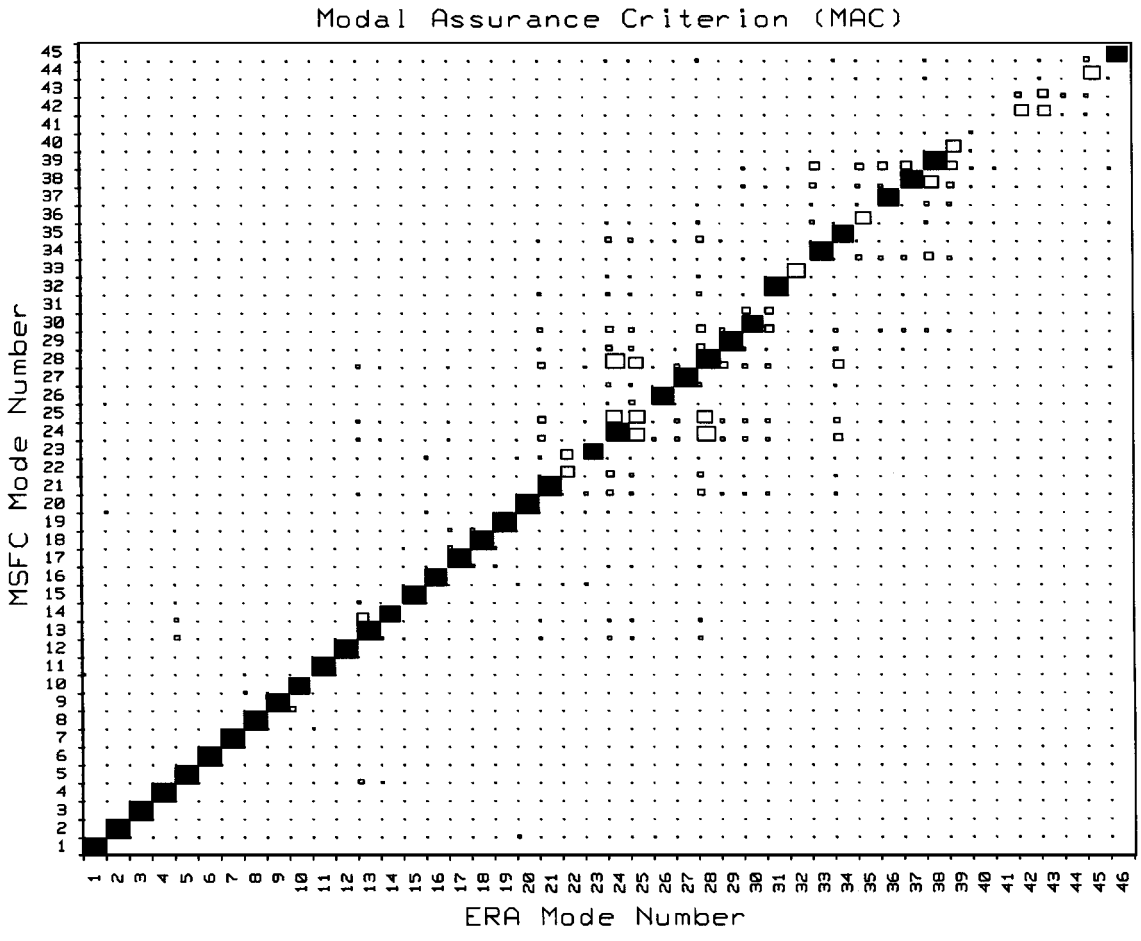

Fig. 7 Correlation of ERA and MSFC mode shapes using MAC; MAC values of 80% or greater are darkened.

axis. Similarly, a mode with a CMI of 50% has a vertical dash height of one half the distance between minor tic marks on the *y* axis. Therefore, those results appearing as solid vertical lines have higher confidence than those appearing as dashed or dotted lines. (Low confidence normally indicates uncertainty in the calculated damping value, mode shape, or frequency, in that order.) Clearly, these ERA results display a wide range of confidence as a function of the assumed number of modes as well as from mode to mode. This is normal for complex experimental data sets due to a variety of real-world effects including nonlinearity, suboptimal excitation, measurement noise, and closely spaced natural frequencies (particularly if the corresponding mode shapes are similar).

Figure 6 contains a total of 2367 mode estimates. Each mode estimate includes a natural frequency, damping factor, mode shape, and CMI value. Frequency, damping, and CMI are scalar quantities, whereas each mode shape is a 1236-component complex vector. A reliable, automatic procedure has been developed to sift through such large sets of results and extract the best, unique set of modes. This procedure originated as a mode condensation algorithm for autonomous system identification.[6] Application of this condensation algorithm to the data in Fig. 6 resulted in the 46 natural frequencies marked by triangles at the top of the plots. The results are also listed in Table 1, including the corresponding damping factors, CMI values, and weighted modal phase collinearity (MPC-W). As mentioned earlier, CMI is the principal ERA accuracy indicator. It normally provides a reliable, single measure of accuracy for each mode. MPC-W supplements CMI and indicates the nearness of the mode shape to a monophase vector, i.e., to a classical normal mode.[8] Values greater than 95% are extremely high. High MPC-W values are particularly meaningful, and harder to achieve, when there are many response measurements. In this application, 29 of 46 modes (63%) have values of 95% or greater.

The ERA analysis shown in Fig. 6 required a few hours of CPU time on a UNIX workstation using a Fortran implementation. The mode condensation procedure that extracted the 46 best, unique modes from the total set of 2367 mode estimates required several additional minutes of computer time. These two steps ran sequentially with only a slight amount of user interaction necessary, i.e., almost autonomously.

Comparison of Results

This section compares the ERA results in Table 1 with the MSFC results given in their test report.[4] First, the mode shapes are compared using the modal assurance criterion (MAC).[9] MAC is the square of the inner product of normalized (unit length) mode-shape vectors. This is the same parameter referred to in statistics as the square of the correlation coefficient. Values greater than approximately 80% indicate a high degree of similarity. Second, the natural frequencies and damping factors of the correlated pairs of ERA and MSFC modes are compared, and the differences are plotted vs mode number.

Figure 7 shows the correlation of all ERA-identified modes with all MSFC-identified modes using MAC. The plot has a simple graphical format as follows. Each row and column represents one mode. The MAC value for each pair of modes is proportional to the size of the rectangle drawn at the intersection of the corresponding row and column. For example, ERA mode 22 and MSFC mode 22 have a MAC value of 55%, and the corresponding intersection contains a rectangle whose width and height are 55% of the *x* and *y* dimensions of the intersection, respectively. Values of 80% or greater are darkened for emphasis.

Figure 7 indicates a very good, one-to-one correspondence of the majority of ERA and MSFC mode shapes. In particular, the first 21 pairs of modes from the two independent data analyses are essentially identical. All of these MAC values are extremely high, above 95%, except modes 10 (87%), 14 (85%), and 16 (92%). Modes 22 and higher show greater deviation from unique, one-to-one correlation. However, the overall similarity of the two sets of

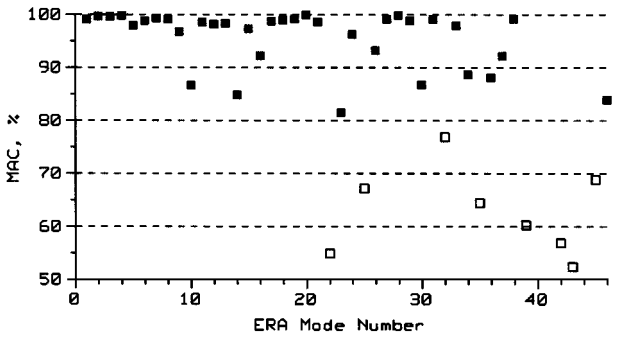

a) Modal assurance criteria (similarity of mode shapes)

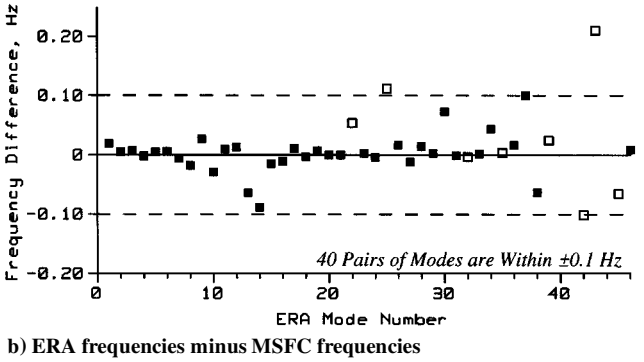

b) ERA frequencies minus MSFC frequencies

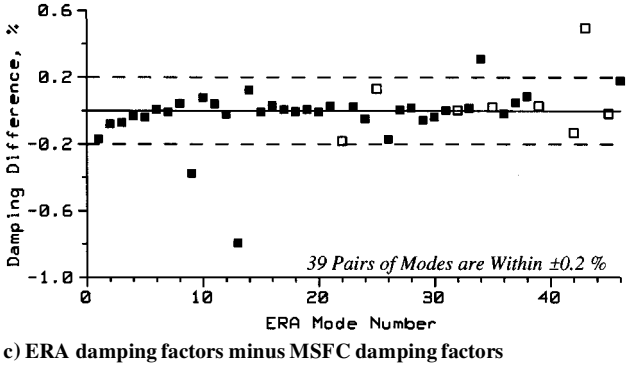

c) ERA damping factors minus MSFC damping factors

Fig. 8 Comparison of ERA and MSFC mode shapes, frequencies, and damping; mode pairs with MAC of 80% or greater are darkened.

with MAC values of at least 80% are darkened in all three plots. This was done to investigate if low MAC values correlate with large frequency and/or damping differences. Surprisingly, there is not a significant trend of this type. For example, although the three largest frequency differences in Fig. 8b occur for modes with MAC values below 80%, three other modes with values below 80% have frequency differences less than 0.025 Hz. Similarly, Fig. 8c shows no consistent trend of low MAC values with large damping differences. Overall, there is excellent agreement of the ERA and MSFC natural frequencies and damping factors, with 40 pairs of modes having a frequency difference of less than 0.1 Hz and 39 pairs of modes having a damping difference of less than 0.2%.

Conclusions

This paper compared independent modal identification results for the space station resource node obtained at NASA LaRC using ERA and at NASA MSFC using commercial software. The resource node is the first U.S.-built structure for the ISS. Each organization analyzed a large set of 3708 FRFs (3 shakers and 1236 accelerometers), with approximately 45 modes of vibration in the test bandwidth of 0 to 50 Hz. The ERA analysis and mode condensation procedure required a few hours of CPU time on a UNIX workstation, and they ran sequentially with only a slight amount of user interaction necessary, i.e., almost autonomously. Overall, there was excellent similarity of mode shapes, natural frequencies, and damping factors for the majority of ERA- and MSFC-calculated modes. This correlation of independent results allows the analytical model validation effort for the space station resource node to proceed with increased confidence in the accuracy and completeness of the experimental modal parameters.

Appendix: Data Analysis Procedure

This appendix documents the specific ERA parameters used to generate the identified natural frequencies (and associated damping factors and mode shapes) shown in Fig. 6.

ERA uses impulse response time histories simultaneously for m initial conditions (inputs), p response locations (outputs), and $k_{\max}$ time samples $y_{ij}(k)$, for $i = 1, 2, \ldots, p$, $j = 1, 2, \ldots, m$, and $k = 1, 2, \ldots, k_{\max}$. In this application, $m = 3$, $p = 1236$, and $k_{\max} = 123$. The data sampling interval Δt is 7.8125 ms, so that the total length of data used in the analysis was $122 \times 0.0078125 = 0.95$ s. The impulse response functions were created by inverse Fourier transformation of experimental FRFs.

Construct two generalized Hankel matrices, $H(0)$ and $H(1)$, using the impulse response data, as follows:

$$H(K) = \begin{bmatrix} Y_1(K+1) & Y_1(K+2) & \cdots & Y_1(K+t) & Y_1(K+t+\Delta C) \\ Y_2(K+2) & Y_2(K+3) & \cdots & Y_2(K+t+1) & Y_2(K+t+1+\Delta C) \\ \vdots & \vdots & \ddots & \vdots & \vdots \\ Y_2(K+s) & Y_2(K+s+1) & \cdots & Y_2(K+s+t-1) & Y_2(K+s+t-1+\Delta C) \\ Y_2(K+s+\Delta R) & Y_2(K+s+1+\Delta R) & \cdots & Y_2(K+s+t-1+\Delta R) & Y_2(K+s+t-1+\Delta R+\Delta C) \end{bmatrix}$$

results is still very good all the way up to ERA mode 39 at 46.7 Hz. Of 25 high-frequency modes starting at mode 22, 14 (56%) have excellent MAC values of 80% or greater.

The 21 low-frequency modes with high MAC values (up to 34.5 Hz) are the most significant from a loads and deformation standpoint. The analytical transient analysis for structural verification of Shuttle payloads uses all modes of the combined Shuttle/payload model up to 35 Hz (Ref. 1). Of course, because some modes of the payload above 35 Hz may drop below this frequency when it is combined with the Orbiter, the recommended goal is to obtain test-verified payload models up to 50 Hz.

Figure 8 shows the MAC, frequency difference, and damping difference of each pair of correlated modes. The 35 pairs of modes

for $K = 0$ and 1. In this application, $s = 4$, $t = 99$, and $\Delta R = \Delta C = 10$. Matrices $H(0)$ and $H(1)$ contain n_r rows and n_c columns, where $n_r = 6180$ and $n_c = 300$. With this arrangement of data, ERA can identify a maximum of $M = \min(n_r, n_c)/2 = 150$ modes.

Submatrix $Y_1(k)$ contains response data for all m inputs and all p outputs at time instant k arranged as follows:

$$Y_1(k) = \begin{bmatrix} y_{11}(k) & y_{12}(k) & \cdots & y_{1m}(k) \\ y_{21}(k) & y_{22}(k) & \cdots & y_{2m}(k) \\ \vdots & \vdots & \ddots & \vdots \\ y_{p1}(k) & y_{p2}(k) & \cdots & y_{pm}(k) \end{bmatrix}$$

Submatrix $Y_2(k)$ is identical to $Y_1(k)$ except with the possible deletion of certain rows. In this application, this row-deletion option was not used; therefore, $Y_2(k) = Y_1(k)$.

Note that every block row and column of $H(K)$ is shifted by one time sample from the previous block row and column, except for the last block row and column. [The $Y_1(k)$ and $Y_2(k)$ submatrices constitute the various block rows and block columns of $H(K)$.] The last block row and column are shifted by 10 time samples from the previous row and column, i.e., $\Delta R = \Delta C = 10$. This additional shifting is done to compute CMI values.[8]

Calculate the singular value decomposition of $H(0)$ as

$$H(0) = PDQ^T$$

where the diagonal matrix D contains the $2M$ singular values of $H(0)$ arranged in order of decreasing magnitude, the columns of P contain the corresponding left singular vectors, and the rows of Q^T contain the corresponding right singular vectors. With ideal, noise-free data having N modes (N must be $\leq M$), there are exactly $2N$ nonzero singular values. With experimental data, however, all of the singular values will normally be nonzero, and it is usually impossible to determine the exact number of modes simply by examining the magnitudes of the singular values. In practice, the assumed number of modes is usually incremented over a range of values, and the corresponding modal parameters and accuracy indicators are compared. The assumed number of modes equals one-half the number of retained singular values, n. In this application, n increments from 4 to 300 in steps of 4, corresponding to an assumed number of modes ranging from 2 to 150 in steps of 2. These are the 75 sets of results shown in Fig. 6.

Let the diagonal matrix D_n contain the n largest singular values, the matrix P_n contain the corresponding columns of P, and the matrix Q_n^T contain the corresponding rows of Q^T. Develop an nth-order ERA state-space realization as follows:

$$A = D_n^{-\frac{1}{2}} P_n^T H(1) Q_n D_n^{-\frac{1}{2}}$$

$$B = D_n^{\frac{1}{2}} Q_n^T(:, m), \qquad C = P_n(p, :) D_n^{\frac{1}{2}}$$

where $(:, m)$ and $(p, :)$ indicate the first m columns and the first p rows of the corresponding matrices.

Transform this realization to modal coordinates using the eigenvector matrix Ψ of A,

$$A' = \Psi^{-1} A \Psi = Z \text{ (diagonal)}$$

$$B' = \Psi^{-1} B, \qquad C' = C\Psi$$

In practice it is not necessary to form the $\Psi^{-1} A \Psi$ matrix product because $A' = Z$, the eigenvalues of A.

The modal damping rate σ_i and damped natural frequency ω_{di} of mode i in rad/s are the real and imaginary parts of the eigenvalues after transformation back to the continuous domain as follows:

$$s_i = \sigma_i \pm j\omega_{di} = \frac{\ln(z_i)}{\Delta t}$$

Modal damping factors (fractions of critical damping) and damped natural frequencies in hertz are as follows:

$$\zeta_i = -\frac{\sigma_i}{\sqrt{\sigma_i^2 + \omega_{di}^2}} (\times 100\%), \qquad f_{di} = \frac{\omega_{di}}{2\pi}$$

Modal participation factors and mode shapes are the corresponding rows of B' and columns of C', respectively.

Acknowledgments

The author thanks Danny Coleman, Blaine Anderson, Kathy Chandler, and Tim Driskill of MSFC and Byron Calvert, Ed Phillips, Steve Woletz, Conrad Ball, and Steve Radke of Boeing for their assistance and support in this cooperative effort.

References

[1] Lambert, C. H., Jr., "Payload Verification Requirements," Space Shuttle Program, NASA Johnson Space Center Rept. NSTS 14046, rev. C, Houston, TX, April 1994.

[2] Foster, R. M., "Structural Design and Verification Requirements," International Space Station Program, NASA Johnson Space Center Rept. SSP 30559, rev. B, Houston, TX, June 1994.

[3] Chandler, K. O., Anderson, J. B., Coleman, A. D., and Driskill, T. C., "Modal Testing of the International Space Station Resource Node," *Proceedings of the 16th International Modal Analysis Conference* (Santa Barbara, CA), Society for Experimental Mechanics, Bethel, CT, 1998, pp. 77–82.

[4] Anderson, J. B., Chandler, K. O., Driskill, T. C., and Coleman, A. D., "ISS Resource Node Fixed Base Modal Survey Test Report," NASA Marshall Space Flight Center Rept. SS-DEV-ED96-112, Huntsville, AL, Feb. 1997.

[5] Juang, J.-N., and Pappa, R. S., "An Eigensystem Realization Algorithm for Modal Parameter Identification and Model Reduction," *Journal of Guidance, Control, and Dynamics*, Vol. 8, No. 5, 1985, pp. 620–627.

[6] Pappa, R. S., Woodard, S. E., and Juang, J.-N., "The Development of Autonomous Structural Modal Identification," *Sound and Vibration*, Vol. 31, No. 8, 1997, pp. 18–23.

[7] Williams, R., Crowley, J., and Vold, H., "The Multivariate Mode Indicator Function in Modal Analysis," *Proceedings of the 3rd International Modal Analysis Conference* (Orlando, FL), Union College, Schenectady, NY, 1985, pp. 66–70.

[8] Pappa, R. S., Elliott, K. B., and Schenk, A., "Consistent-Mode Indicator for the Eigensystem Realization Algorithm," *Journal of Guidance, Control, and Dynamics*, Vol. 16, No. 5, 1993, pp. 852–858.

[9] Allemang, R. J., and Brown, D. L., "A Correlation Coefficient for Modal Vector Analysis," *Proceedings of the 1st International Modal Analysis Conference* (Orlando, FL), Union College, Schenectady, NY, 1982, pp. 110–116.